*Inorg. Chem.* **2009**, *48*, 879−888

# α- to β-(dmes)$BiI_5$ (dmes = Dimethyl(2-ethylammonium)sulfonium Dication): Umbrella Reversal of Sulfonium in the Solid State and Short I···I Interchain Contacts—Crystal Structures, Optical Properties, and Theoretical Investigations of 1D Iodobismuthates

**Nicolas Louvain,[†] Nicolas Mercier,*[,†] and Florent Boucher[‡]**

*Laboratoire de Chimie et Ingénierie Moléculaire d'Angers, UMR-CNRS 6200, Université d'Angers 2 Bd Lavoisier, 49045 Angers, France, and Institut des Matériaux Jean Rouxel, UMR-CNRS 6502, Université de Nantes, 2 rue de la Houssinière, BP 32229, 44322 Nantes Cedex 3, France*

Received July 31, 2008

Syntheses, X-ray structural characterization, optical properties, and electronic structures of 1D metal(III) iodide hybrids, namely, α-$((CH_3)_2S(CH_2)_2NH_3)BiI_5$ (**1a**), β-$((CH_3)_2S(CH_2)_2NH_3)BiI_5$ (**1b**), $((CH_3)_2S(CH_2)_2NH_3)SbI_5$ (**2**), and $(HO_2C(C_6H_4)CH_2NH_3)BiI_4$ (**3**), are reported. According to the results of single-crystal X-ray diffraction analyses, the 1D inorganic chains are constructed by corner-shared M(III)$I_6$ octahedra in **1a**, **1b**, and **2** and by edge-shared ones in **3**. In polymorphs **1a**, **1b**, and **2**, the polymeric $BiI_5^{2-}$ anionic chains are charge-balanced by the dimethyl(2-ethylammonium)sulfonium (dmes) dications. Complex **1a** crystallizes in the polar space group of $P2_1cn$. A spectacular umbrella reversal of half sulfonium parts together with the conformational change of half polymeric anions in the crystal structure of **1a** occurs at moderate temperature (73 °C), leading to the β-phase **1b**, through a reversible single-crystal-to-single-crystal process. Complex **1b**, as well as the isotype structure of **2**, crystallize in the nonpolar acentric space group of $P2_12_12_1$. Because of their acentric structural characteristic, second harmonic generation (SHG) optical properties are observed in the polycrystalline powder samples of **1a**, **1b**, and **2**. It is notable that the SHG signal of **1a** is much stronger than that of **1b** and **2** owing to the polarity of **1a**. Remarkably, the peculiar dissymmetrical dication of dmes is able to modify the bonding features of the inorganic frameworks through shortening I···I distances between adjacent chains ($d$(I···I) < 4Å). The structure of **3**, which crystallizes in the triclinic space group $P\bar{1}$, features a polymeric anionic chain constructed from edge-shared $BiI_6$ octahedra. The charge is balanced by the pairs of *trans*-4-(ammoniummethyl)-cyclohexane-carboxylic acid, which are linked together via the H bonding between the carboxylic groups to form a pseudodication. The results of DFT calculations based on the structures of **1a** and **3** indicate that the narrower band gap in **1** appears to be associated on the one hand with a σ* I-p/Bi-s interaction that moves the Fermi level to higher energy and on the other hand with the interchain I···I contacts.

## Introduction

At present, one of the most successful strategies to obtain novel functional materials is to combine the specific properties of the inorganic frameworks, such as electronic properties, and the intriguing features of the organic ligands, such as flexibility and the ability to form weak interactions. Among all kinds of hybrids, the halogenometallate salts are of importance not only because of their interesting magnetic, optical, and electrical properties mainly arising from the inorganic frameworks[1] but also because of their good solubility at room temperature.[2] As a consequence, quite a number of halogenometallate hybrids can be easily processed into nice thin films using the spin-coating technique to form electronic or optoelectronic devices. For example, in the distinguished hybrid of $(C_6H_5C_2H_4NH_3)_2SnI_4$,[3] the electrical mobility is up to 0.6 $cm^2\ V^{-1}\ s^{-1}$, which makes it a good candidate for the semiconducting channel in field-effect

* To whom correspondence should be adressed. Tel.: 33.(2).41.73.50.83. Fax: 33.(2).41.73.54.05. E-mail: nicolas.mercier@univ-angers.fr.
† Université d'Angers 2 Bd Lavoisier.
‡ Université de Nantes.

(1) Mitzi, D. B. *Prog. Inorg. Chem.* **1999**, *48*, 1–121.
(2) (a) Mitzi, D. B. *Chem. Mater.* **2001**, *13*, 3283. (b) Mitzi, D. B. *J. Mater. Chem.* **2004**, *15*, 2355.

10.1021/ic801900r CCC: $40.75 
Published on Web 12/31/2008

transistors.[3a] The 2-D nature of the inorganic network and suitable bonding features in perovskite layers are key factors influencing semiconducting properties.[1,4,5]

Owing to their potential semiconducting properties, hybrids of iodobismuthates have already absorbed much attention from material chemists. To date, there are more than 60 iodobismuthate complexes that have been reported (Cambridge Structural Database, version 5.29, Nov. 2007). In most cases, the inorganic frameworks are discrete clusters ranging from $BiI_6^{3-}$ [6] to $Bi_8I_{30}^{6-}$.[7] As the cluster size increases, the band gaps between VB and CB in these hybrids are greatly reduced, which can be validated by the trend of color changing from orange ($BiI_6^{3-}$) to dark red ($Bi_8I_{30}^{6-}$). Unfortunately, the corresponding salts built up from isolated clusters exhibit poor electronic properties.[8] Of all iodobismuthate hybrids, those based on higher dimensionality anionic frameworks are promising candidates for semiconducting materials. In order to increase the dimensionality of the inorganic network, transition metal ions, such as $Ag^+$ or $Cu^+$, have been introduced into these systems to link the adjacent clusters into infinite chains[9] or layers.[9b] However, these monovalent cations are not suitable bridges to transfer electrons between bismuth entities. To the best of our knowledge, hybrid iodobismuthate with a 2D extended anionic framework is very rare since only one structure, namely $[Bi_{2/3}I_4^{2-}]_n$, has been reported in which the deficient anionic layers are stabilized by quaterthiophene cations,[10] whereas structures of 1D infinite chains, $[Bi_2I_7^{2-}]_n$,[11] $[Bi_3I_{11}^{2-}]_n$,[11b,12] $[BiI_4^-]_n$,[13] and $[BiI_5^{2-}]_n$,[14] are comparatively common. As is well-known, it is still a great challenge to control the structures or the dimensionalities of metal−halide anionic frameworks. The structure varies depending on the experimental conditions, such as the solvent, ratio of reagents, and temperature, as well as the features of the counterions, such as size, charge, and conformation. Generally, the trend is that nonbulky ligands with a higher charge density such as the primary ammonium group, which is able to form H bonds with the terminal I atoms, lead to anions with high I/M ratios, as in the case of 1D $M^{III}I_5^{2-}$ or 2D $M^{II}X_4^{2-}$. Except for increasing the dimensionality of the inorganic frameworks, another successful strategy for lowering the band gap is the incorporation of multifunctional organic cations able to impact the bonding features within the inorganic network[5] as well as to enhance the orbital interaction across adjacent chains.[15] Although a large spectrum of cations, mainly ammonium (from primary to quaternary type), but also quaternary phosphonium, and more recently metal−organic coordination complexes,[16] have already been investigated, only one alkylsulfonium-based iodometallate hybrid has been reported.[17]

In this article, the synthesis and single-crystal structures of four metal(III) iodide hybrids with one-dimensional inorganic frameworks, α-$((CH_3)_2S(CH_2)_2NH_3)BiI_5$ (**1a**), β-$((CH_3)_2S(CH_2)_2NH_3)BiI_5$ (**1b**), $((CH_3)_2S(CH_2)_2NH_3)SbI_5$ (**2**), and $(HO_2C(C_6H_4)CH_2NH_3)BiI_4$ (**3**), are reported. The peculiar asymmetrical dication of dimethyl(2-ethylammonium)sulfonium (dmes), with polar sulfonium and primary ammonium groups in one entity, is incorporated in the acentric crystal structures of **1a** and **2**. We will show that the acentric polar **1a** compound can reversibly be transformed into the corresponding acentric apolar β-phase **1b**, which is isotypical to **2**, via a single-crystal-to-single-crystal process occurring upon heating at 73 °C, due to an umbrella reversal of one-half of the sulfonium groups. We will also show that another impact of the dmes dications on structures is the shortening of I···I interchain distances ($d_{I...I} < 4$ Å), which modulates the electronic properties of hybrids. Finally, electronic structures of **1a** will be investigated and discussed through a study at the DFT level of theory and then compared to the one of **3** having a structure based on the other common type of iodobismuthate chain, $BiI_4^-$, constructed by edge-shared $BiI_6$ octahedra. In order to elucidate the density of states (DOS) and band gap related to these pnictogen-based hybrids, calculations on a series of model compounds have also been carried out in order to determine the influence of the nonbonded I···I interaction.

## Experimental Section

**Synthesis and Thermal Characterization. Complexes 1a and 2.** These compounds were prepared by the solvothermal method using a Teflon-lined PARR autoclave (internal volume 25 mL). To 0.6 mmol of $M^{III}I_3$ (99%; M = Bi, MW = 589.69, 353.81 mg; M = Sb, MW = 502.46, 301.47 mg) and 0.3 mmol of cystamine dihydrochloride (97%, MW = 225.2, 67.56 mg) were added 4 mL of methanol and 3.96 mL of hydriiodic acid (MW = 127.91, 57 wt %, $d$ = 1.7, 30 mmol). The autoclave was heated in a programmable oven with the following parameters: 2 h heating from 25 to 85 °C, 2 h remaining at 85 °C, then 12 h cooling down to 25


(3) (a) Kagan, C. R.; Mitzi, D. B.; Chondroudis, K. *Sciences* **1999**, *286*, 945. (b) Mitzi, D. B.; Chondroudis, K.; Kagan, C. R. *IBM J. Res. Dev.* **2001**, *45* (1), 29.
(4) Knutson, J. L.; Martin, J. D.; Mitzi, D. B. *Inorg. Chem.* **2005**, *44*, 4699.
(5) Sourisseau, S.; Louvain, N.; Bi, W.; Mercier, N.; Rondeau, D.; Boucher, F.; Buzaré, J. Y.; Legein, C. *Chem. Mater.* **2007**, *19*, 600.
(6) Lindsjö, M.; Fischer, A.; Kloo, L. *Z. Anorg. Allg. Chem.* **2005**, *631*, 1497.
(7) Feldmann, C. *J. Solid State Chem.* **2003**, *172*, 53.
(8) Gridunova, G. V.; Ziger, E. A.; Koshkin, V. M.; Struchkov, Y. T.; Shklover, V. E. *Zh. Neorg. Khim.* **1988**, *33*, 1718.
(9) (a) Chai, W.-X.; Wu, L.-M.; Li, J.-Q.; Chen, L. *Inorg. Chem.* **2007**, *46*, 1042. (b) Feldmann, C. *Inorg. Chem.* **2001**, *40*, 818.
(10) Mitzi, D. B. *Inorg. Chem.* **2000**, *39*, 6107.
(11) (a) Rogers, R. D.; Bond, A. H.; Aguinaga, S.; Reyes, A. *J. Am. Chem. Soc.* **1992**, *114*, 2967. (b) Krautcheild, H. *Z. Anorg. Allg. Chem.* **1995**, *621*, 2049.
(12) Goforth, A. M.; Peterson, L. P., Jr.; Smith, M. D.; zur Loye, H. C. *J. Solid State Chem.* **2005**, *178*, 3529.
(13) (a) Chaabouni, S.; Kamoun, S.; Jaud, J. *J. Chem. Crystallogr.* **1997**, *27*, 727. (b) Bowmaker, G. A.; Junk, P. C.; Lee, A. M.; Skelton, B. W.; White, A. H. *Aus. J. Chem.* **1998**, *51*, 293.
(14) (a) Mousdis, G. A.; Papavassiliou, G. C.; Terzis, A.; Raptopoulou, C. P. *Z. Naturforsch.* **1998**, *53b*, 927. (b) Mitzi, D. B.; Brock, P. *Inorg. Chem.* **2001**, *40*, 2096. (c) Goforth, A. M.; Smith, M. D.; Peterson, L., Jr.; zur Loye, H. C. *Inorg. Chem.* **2004**, *43*, 7042. (d) Bi, W.; Louvain, N.; Mercier, N.; Luc, J.; Rau, I.; Kajzar, F.; Sahraoui, B. *Adv. Mater.* **2008**, *20*, 1013.
(15) Xu, Z.; Mitzi, D. B.; Dimitrakopoulos, C. D.; Maxcy, K. R. *Inorg. Chem.* **2003**, *42*, 2031.
(16) (a) Krautcheild, H. *Z. Anorg. Allg. Chem.* **1994**, *620*, 1559. (b) Tershansy, M. A.; Goforth, A. M.; Peterson, L., Jr.; Burns, M. C.; Smith, M. D.; zur Loye, H. C. *Solid State Sci.* **2007**, *9*, 895.
(17) Paulsson, H.; Berggrund, M.; Fischer, A.; Kloo, L. *Eur. J. Inorg. Chem.* **2003**, 2352.

**Table 1.** Crystallographic Data for **1a, 1b**, **2**, and **3**: α- and β-(dmes)$BiI_5$, (dmes)$SbI_5$, and $(HO_2C-C_6H_4-CH_2NH_3))BiI_4$, Respectively

| | 1a | 1b | 2 | 3 |
|---|---|---|---|---|
| fw (g/mol) | 950.69 | 950.69 | 863.46 | 873.79 |
| space group | $P2_1cn$ | $P2_12_12_1$ | $P2_12_12_1$ | $P\bar{1}$ |
| *a*, Å | 8.4752(3) | 8.5334(2) | 8.4951(10) | 8.1071(16) |
| *b*, Å | 12.6137(15) | 12.732(1) | 12.8193(15) | 9.871(2) |
| *c*, Å | 16.385(2) | 16.195(2) | 15.694(2) | 12.271(3) |
| α, deg | 90 | 90 | 90 | 68.97(3) |
| β, deg | 90 | 90 | 90 | 83.37(3) |
| γ, deg | 90 | 90 | 90 | 83.48(3) |
| *V*, Å$^3$ | 1751.6 | 1759.5(3) | 1709.1(4) | 907.7(3) |
| *Z* | 4 | 4 | 4 | 2 |
| obsd reflns ($I > 2\sigma(I)$) | 4664 [0.078] | 3849 [0.038] | 4944 (0.034) | 5280 (0.048) |
| params | 110 | 110 | 109 | 146 |
| Flack param | 0.26(1) | 0.48(1) | 0.00(6) | |
| R1($I > 2\sigma(I)$)/ wR2(all data) | 0.033/0.0604 | 0.031/0.0503 | 0.032/0.0578 | 0.041/0.0924 |

°C. Dark red crystals were collected by filtration and washed with cold ethylacetate (yield 70−80% on the basis of $M^{III}I_3$). The dmes dication is formed in situ by the reaction of cystamine and $CH_3I$, this last coming from the reaction of methanol and HI (the presence of $CH_3I$ has been proved by a $^1$H NMR spectrum of the filtrate δ 2.16 ppm). Anal. calcd for **1a** (dried): C, 5.05; H, 1.38; N, 1.47; S, 3.38; Bi, 21.98; I, 66.74. Found: C, 5.07; H, 1.32; N, 1.51; S, 2.99; Bi, 24.93; I, 64.04. Anal. calcd for **2** (dried): C, 5.56; H, 1.52; N, 1.62; S, 3.72; Sb, 14.10; I, 73.48. Found: C, 5.62; H, 1.49; N, 1.66; S, 3.36; Sb, 13.40; I, 72.80.

**Complex 3.** $BiI_3$ (0.1200 g, 0.20 mmol, 99%) and *trans*-4-(aminomethyl)-cyclohexane-carboxylic acid (0.0478 g, 0.30 mmol, 97%) were dissolved into 25 mL of an EtOH and $H_2O$ solvent mixture (1.5:1). Then, 0.25 mL of concentrated HI (57 wt %) was added to the solution in drops under stirring. Before being put in a ventilating cabinet, the solution was heated for 1 h near reflux. Small prismatic red (main phase) and orange crystals were collected after 24 h; two kinds of samples were separated by hand-picking under the microscope.

X-ray powder patterns of the homogeneous samples of **1a**, **1b**, **2**, and **3** showed that all of the observed reflections were fully indexed using the unit cell parameters obtained from single-crystal X-ray diffraction experiments (Supporting Information).

Differential scanning calorimetry (DSC) and thermogravimetric analysis (TGA) were performed on the DSC-2010 and TGA-2050 TA Instruments systems in the laboratory ranging from 20 to 350 °C and 20−900 °C, respectively (see the Supporting Information). The first weak endothermic peak in the DSC curve of **1a** ($T = 73$ °C) corresponds well to the phase transformation from **1a** to **1b**, and the reversibility has been checked (see text). Above 73 °C, the β-phase **1b** is then stable up to 190 °C before decomposition in two close steps in the 190−360 °C range. Complex **2** is stable up to 200 °C (melting) and then rapidly decomposes in two steps up to 400 °C. Complex **3** is stable up to 250 °C, and then rapidly decomposes in one step.

**X-Ray Crystallography.** X-ray powder diffraction measurements were carried out on a D8 Bruker diffractometer using Cu $K\alpha_{1,2}$ radiation, equipped with a linear Vantec super-speed detector and a TTK450 temperature chamber. X-ray diffraction data of selected single crystals were collected on a Bruker-Nonius KAPPA-CDD diffractometer equipped with graphite-monochromated Mo Kα radiation ($\lambda = 0.71073$Å) at $T = 293$ K (**1a**, **2**, **3**) and at $T = 353$ K (**1b**) using an Oxford cryosystem (liquid nitrogen cryostream working in the range 100−470 K). A summary of crystallographic data and refinement results for all compounds is listed in Table 1. Structures were solved and refined using the Shelxl97 package. Heavy atoms (Bi, Sb, I, S) were first located using direct methods, C and N atoms being then located from the analysis of the Fourier difference maps. Positions and atomic displacement parameters were refined by full-matrix least-squares routines against $F^2$. All hydrogen atoms were treated with a riding model in all four structures. Refinements of positions and anisotropic displacement parameters of all non-H atoms lead to $R = 0.033$, $R = 0.031$, $R = 0.032$, and $R = 0.041$ for **1a, 1b**, **2**, and **3**, respectively. A complete list of crystallographic data, along with the atomic coordinates, the anisotropic displacement parameters, and bond distances and angles for each compound, are given as Supporting Information.

**NLO Measurements.** The crystals of **1a**, **2**, and POM (3-methyl-4-nitropyridine-1-oxide, used as a reference) were crushed and sieved in order to ensure a crystallite size in the range of 125−250 μm and were then placed between two microscope slides. All experiments were carried out under the same conditions; especially and in particular, the same amount of sample was used. The second harmonic generation (SHG) measurements were performed by applying the Kurtz and Perry method[18] (fundamental excitation wavelength at 1064 nm). The power of the fundamental beam was tuned with a half-wave plate and a Glan polarizer. The beam was focused on the sample by a convergent lens with a focus of 250 mm. The SHG signals were detected by a photomultiplier tube (Hamamatsu R1828−01), then integrated by a boxcar integrator, and processed by a computer. For temperature-dependent SHG experiments (**1a**), a heating ramp of 0.3 K/nm was used.

**Electronic Band Structures Calculations.** All calculations and geometry optimizations were carried out at the DFT level of theory using the PBE96[19] functional. In the first step, in order to check the accuracy of the DFT/GGA approach to describe the electronic structure of these hybrid materials, structural optimizations were performed for compounds **1a** and **3** (given as Supporting Information). The two-step approach has already been described elsewhere.[5] Experimental cell parameters being fixed, the internal atomic coordinates of all of the atoms were adjusted, using a VASP package[20] based on the efficient projected augmented wave (PAW) approach,[21] by minimizing Hellmann−Feynman forces. All calculations were converged with regards to the kinetic energy cutoff used for the plane wave basis set expansion and to the *k*-point density needed for the Brillouin zone integration. For the dmes-based compound **1a**, a cutoff of 500 eV and a $(3 \times 3 \times 3)$ Monkhorst−Pack *k*-points mesh were *used* to achieve convergence. A $(5 \times 4 \times 3)$ *k*-points mesh and a cutoff of 500 eV were the parameters used for **3**. The PAW pseudopotential that has been chosen for the VASP calculations uses the following atomic electronic configurations to describe the valence states: Bi ($5d^{10}$ $6s^2$ $6p^3$), I ($5s^2$ $5p^5$), C ($2s^2$ $2p^2$), N ($2s^2$ $2p^3$), S ($3s^2$ $3p^4$), and H ($1s^1$). The accuracy of the optimized bond lengths are discussed in the Supporting Information.

In a second step, electronic structure calculations for the DOS and band dispersion analyses have been made on these optimized structures using the very accurate full potential linearized augmented plane wave (FLAPW) method, as embodied in the WIEN2k

(18) Kurtz, S. K.; Perry, T. T. *J. Appl. Phys.* **1968**, *39*, 3798.
(19) Perdew, J. P.; Burke, S.; Ernzerhof, M. *Phys. Rev. Lett.* **1996**, *77*, 3865.
(20) (a) Kresse, G.; Furthmüller, J. *Comput. Mater. Sci.* **1996**, *6*, 15. (b) Kresse, G.; Furthmüller, J. *Phys. Rev. B: Condens. Matter Mater. Phys.* **1996**, *54*, 11169.
(21) (a) Blöchl, P. E. *Phys. Rev. B: Condens. Matter Mater. Phys.* **1994**, *50*, 17953. (b) Kresse, G.; Joubert, D. *Phys. Rev. B: Condens. Matter Mater. Phys.* **1999**, *59*, 1758.

package.[22] This method is often used for the analysis as it offers an easier decomposition of the wave function into atomic-like orbitals. Nevertheless, the WIEN2k code is highly computer-demanding when the structure contains atoms with small radii (C, N, H, etc.). Therefore, only the inorganic part of our hybrids was introduced for the FLAPW calculation. The positive charge bared by organic entities was simulated by placing a sodium atom on the ammonium and sulfonium sites. Benchmarking was done in an earlier study using various methods to simulate the positive charge.[5] For each compound, the DOS and electronic gap obtained with VASP (complete structure) and WIEN2k (inorganic part + sodium) were compared to justify the use of an alkaline metal. For the FLAPW calculation, $R_{MT} \times K_{MAX} = 7.0$ was used to define the size of the basis set, using the following muffin tin radii: $R_{MT}(Bi) = 2.7$ Å, $R_{MT}(I) = 2.5$ Å, and $R_{MT}(Na) = 2.3$ Å. $k$ point densities similar to previous ones were used. For all compounds studied, band structures were calculated along high-symmetry lines, as taken from Bradley and Cracknell.[24] As the sodium 3p orbitals often stand close to the bottom of the conduction band (CB), they were removed from the basis set after the self-consistent field (SCF) convergence in order to clarify the DOS and band structures. No significant effect over the final electronic structure of the inorganic part has been observed.

Furthermore, other calculations were performed on two idealized model compounds: **1a2.5** and **1a5.0**. They were based on the **1a** structure to emphazise the interchain interactions. The cell parameters perpendicular to the chain axis were augmented by 2.5 and 5%, keeping metal−iodide distances identical within a $BiI_5^{2-}$ ribbon but increasing the interchain distances (CIF files given as Supporting Information). Moreover, the parameters used for DOS and band dispersions are the same as for the **1a** compound.

## Results and Discussion

**Synthesis, Crystal Structures and SHG Properties of 1a, 1b, and 2.** Crystals of **1a** and **2** are synthesized under solvothermal conditions (methanol solution) from $M^{III}I_3$ (M = Bi, Sb), cystamine dihydrochloride, and hydriiodic acid as starting materials. The dmes dication is formed in situ through the nucleophilic attack of $CH_3I$ by cystamine, the iodomethane molecules resulting from the halogenation reaction of $CH_3OH$ by HI.

The crystal structure of **1a** consists of dmes dications and $BiI_{4/2}I_{2/2}^{2-}$ polymeric anionic chains of cis-corner-shared $BiI_6$ octahedra. As appreciated when being viewed along the inorganic chain axis (Figure 1), one polymeric anion is, when considering their $BiI_3$ equatorial plane, perpendicular to the four neighboring chains, and the space between four adjacent chains is occupied by dmes pairs, which are marked by black circles in Figure 1. When the temperature is up to 75 °C, the single crystal of **1a** can be transformed into its $\beta$-phase **1b**, via a reversible single-crystal-to-single-crystal process. The reversibility of the transition is confirmed by DSC experiments (Figure 2) as well as by X-ray single-crystal

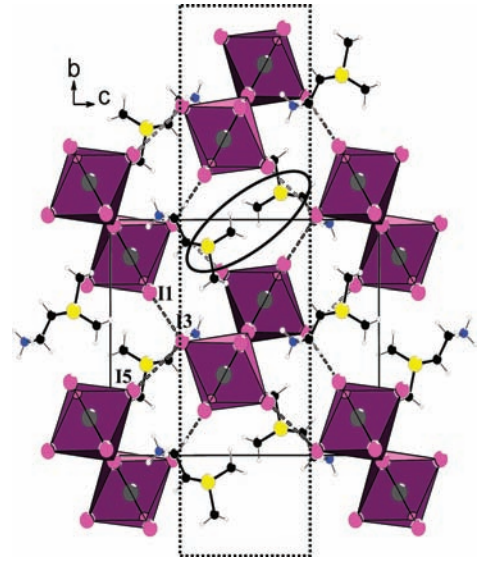


**Figure 1.** Structures of **1a** viewed along the $BiI_5$ chain direction showing the I···I interchain contacts (dashed lines). The circle underlines pairs of molecular entities encaged between four adjacent $BiI_5$ chains while the rectangle (dotted line) underlines a sheet parallel to (a, b) in which polymeric anions and cationic parts remain nearly unchanged through the structural transition at 75 °C.

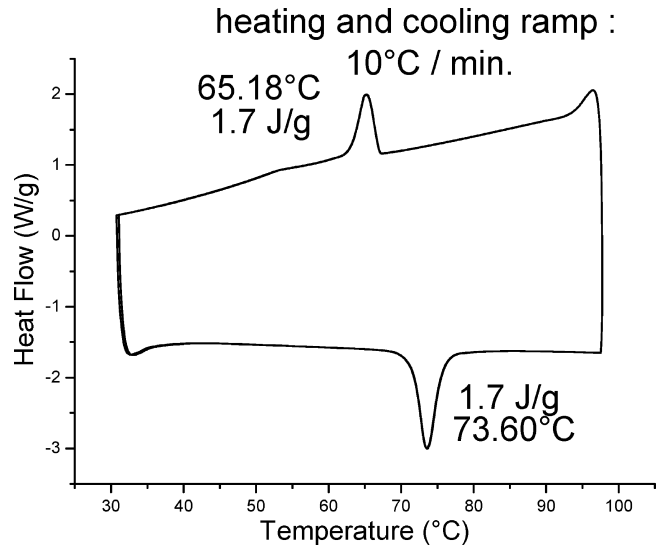


**Figure 2.** DSC experiment of sample **1a** showing the reversibility of the structural transition.

and X-ray powder experiments (Supporting Information). The space group of **1b** is $P2_12_12_1$, which is nonpolar and acentric. It means that the polarity of **1a** has been canceled during the transition. It is remarkable that both the conformation and the arrangement of the dmes molecules in the structure are changed in this process. As shown in Figure 3a, the dmes dications in **1a** adopt the cis conformation related to the C1−C2 bond, and the torsion angle of the N−C1−C2−S part equals 76.9°. Meanwhile, all dipolar moments of sulfonium heads are orientated along the $a$ axis, which is in good accordance with its polar space group of $P2_1cn$. And actually, one can easily see from Figure 3b that half of the sulfonium heads underwent an umbrella reversal in **1b** during the phase transfer, while the orientation of the $CH_2-NH_3^+$ fragment in another half of the dmes cations has also been altered, leading to a nonpolar molecular layout. As a result,

(22) Blaha, P.; Schwarz, K.; Madsen, G. K. H.; Kvaniscka, D.; Luitz, J. *An Augmented Plane Wave + Local Orbitals Program for Calculating Crystal Properties*; Schwarz, K., Ed.; Techn. Universität Austria: Vienna, Austria, 2001; ISBN: 3-9501031-1-2.
(23) (a) Brown, I. D.; Altermatt, D. *Acta Crystallogr.* **1985**, *B41*, 244. (b) Brese, N. E.; O'Keeffe, M. *Acta Crystallogr.* **1991**, *B47*, 192.
(24) Bradley, C. J.; Cracknell, A. P. *The Mathematical Theory of Symmetry in Solids*; Clarendon: Oxford, U.K., 1972.

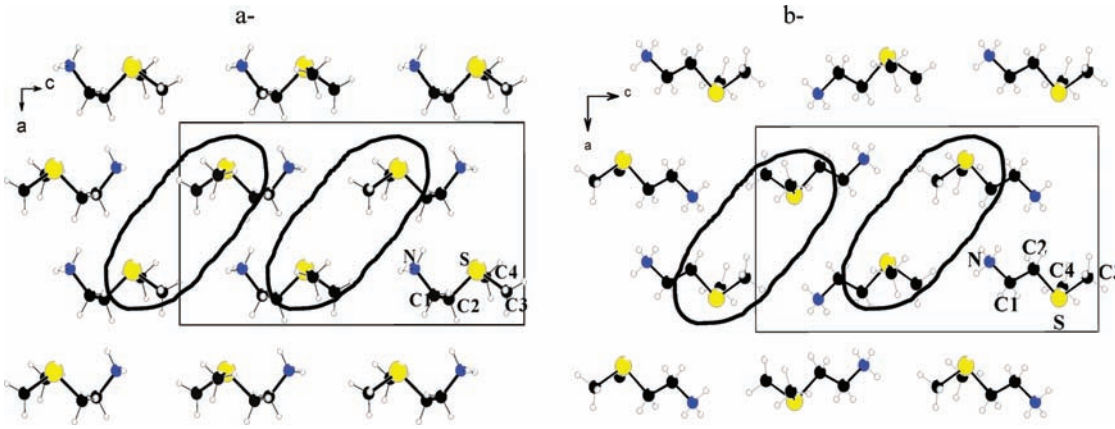


**Figure 3.** View along *b* of the layout of cationic entities in the structures of **1a** (a) and **1b** (b), showing the polar (**1a**) and nonpolar (**1b**) nature of the molecular packing. The circles underline pairs of molecules defined in Figure 1.

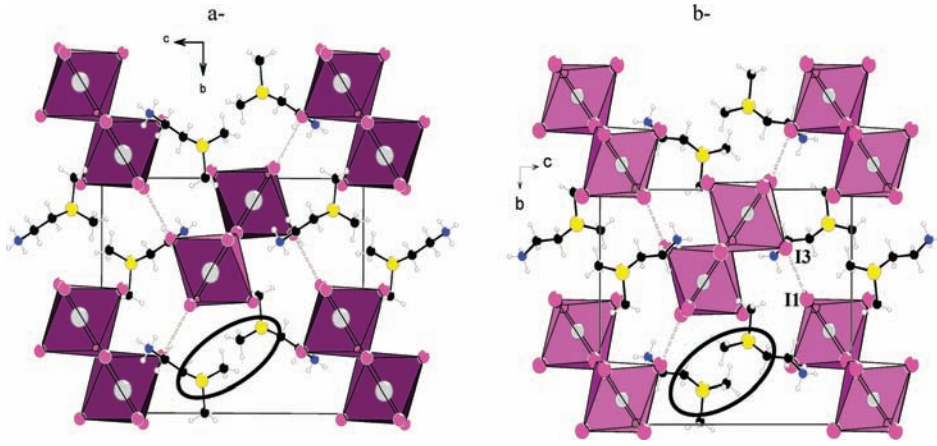


**Figure 4.** Isotype structures of **1b** and **2** viewed along the inorganic chains' axis. The circle underlines pairs of molecular entities encaged between four adjacent $MI_5$ chains.

the conformation of every dmes cation was changed to trans with the torsion angle of N−C1−C2−S equal to −172.9° (Figure 3b). As previously defined, the relative orientations of sulfonium heads in dmes pairs are kept in the structure of **1b**, certainly as a result of dipolar interactions between them. However, the dmes cations belonging to pairs appear a little interpenetrated in **1b** (Figure 4a), while they are not in **1a** (Figure 1), and this can be related to the longer *b* axis and the shorter *c* axis in **1b** ($b$ = 12.732(1) Å, $c$ = 16.195(2) Å) compared to **1a** ($b$ = 12.6137(15)Å, $c$ = 16.385(2) Å). This structural feature is more distinguishable in the structure of the antimony compound **2** ($b$ = 12.8193(15)Å, $c$ = 15.694(2)Å), which is isostructural to **1b** (Figure 4b). When focusing on the molecular layout in the structures of **1a** and **1b**, it is clear that the cancelation of polarity in **1b** is a global process in which the structures of the inorganic polymeric anions are also involved. And it is worth noting that one of every two chains remains unchanged through the transition, while the other undergoes a conformational change, that is, a rotation of octahedra around the Bi−$I_{apical}$ bond direction (Figure 5). This feature is directly correlated to a positional change of all cationic parts next to such chains. In summary, all polymeric anions and cationic parts belonging to a sheet parallel to (*a*, *b*), as defined in Figure 1 by a rectangle with dotted lines, remain unchanged, while all of those belonging to neighboring sheets undergo a conformational change. This is in good accordance with the fact that only one cationic part of each molecule undergoes a positional change through the transition, as already pointed out.

Second-order nonlinear optical (NLO) properties, which are only available in noncentrosymmetric materials, have been detected on the powder samples of **1a** and **2**. The effective second-order susceptibility tensors were evaluated by using the approximate Kurtz−Perry method.[14] A powder sample of 3-methyl-4-nitropyridine-1-oxide (POM) was used as a reference material to determine the value of SHG efficiency. The value of the second-order nonlinear efficiency of **1a** is 0.20 pm/V (1.6% of POM and 20% of quartz efficiencies), which is much higher than that of **2** (0.05 pm/V). Furthermore, both compounds possess a threshold damage value of 3.5 GW/cm$^2$, which is higher than that of POM (3.0 GW/cm$^2$ for the laser beam with $\lambda$ = 1064 nm). When the sample of **1a** was heated, the intensity of the SHG signal was monotonous up to 75 °C and then decreased abruptly to 25% of the original value (heating speed of 0.3 °C/min, Figure 6a). This result is in good accordance with the phase transition being observed in X-ray diffraction experiments since both **1a** and **1b** are acentric. It is worth noting that the stronger SHG signal in **1a** compared to **1b** and **2** can be attributed to its polarity, while the metal ions, $Bi^{3+}$ and $Sb^{3+}$, have no influence on their NLO properties. Nevertheless, we must note that all of these SHG efficiencies

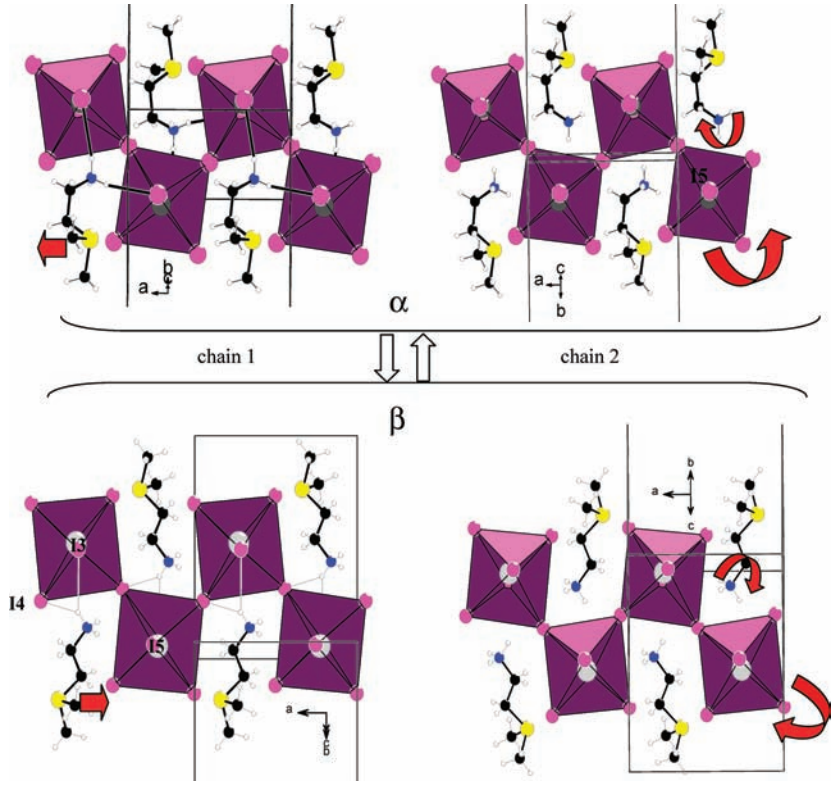


**Figure 5.** Parts of the structure of **1a** (α phase) and **1b** (*β* phase) showing the structural changes that undergo two adjacent chains and the close cationic entities through the reversible α- to *β*-transformation at 75 °C. Arrows indicate the rotation of octahedra along the $I_{apical}-I_{apical}$ direction, as well as the rotation of the ($CH_2NH_3$) fragment and the umbrella reversal of sulfonium parts through the transition.

remain weak, and this is in part due to the absorption of the 532 nm generated light by colored samples (UV−vis spectra of **1a** given in Figure 6b).

As regards the structural characteristics of the $M^{(III)}I_5$ polymeric chains, we first notice that the average Sb−I bond distance ($d$ = 3.026Å, **2**) is shorter than the average Bi−I bonds (3.083Å (**1a**), 3.077 Å (**1b**)), which is congruous with the slightly smaller size of $Sb^{3+}$. Although both of the $MI_6$ polyhedra are distorted from the ideal octahedral geometry, the bonding features of $BiI_6$ and $SbI_6$ octahedra are quite similar, which indicates the weak stereoactivity of lone pairs in both Bi and Sb compounds ($BiI_6$: $d$(Bi−I) in the range of 2.948−3.240Å (**1a**) and 2.911−3.264 Å (**1b**), I−Bi−I bond angles in the range of 83.77−95.90° and 171.43−176.32° (**1a**), and 83.98−93.86° and 165.08−176.82° (**1b**); $SbI_6$: d(I−Sb−I) = 2.841−3.241Å, I−Sb−I, 85.01−92.41° and 175.47−177.81°, respectively (tables given as Supporting Information). The most interesting structural feature is that the shortest distance between two adjacent inorganic chains involving the nearest terminal I atoms is less than 4 Å ($d$(I1···I3) = 3.942(5) Å and $d$(I3···I5) = 3.973(5) Å in **1a** (Figure 1) and $d$(I1···I3) = 3.907(5) Å in **2** (Figure 4b)), which is much shorter than the sum of van der Waals radii of two I atoms (4.3 Å). To the best of our knowledge, such a short distance is unprecedented in the hybrids with a $[M^{III}I_5^{2-}]_n$ network, as well as with the well-known $[M^{II}I_4^{2-}]_n$ network. Other short distances within 4.0−4.3 Å between I atoms from different chains are also being counted in both structures. We speculate that sulfonium heads help to bring adjacent chains closer together.

**Crystal Structure of 3.** During the process of searching for ammonium cations with the ability to influence the configurations of anionic halogenometallate entities as well as to modify the bonding features of a given structure, we recently incorporated bifunctional cations, as amino carboxylic acid molecules. As is well-known, the carboxylic groups from two different molecules incline to link together through the hydrogen bondings in two different modes to form complex ligands, or synthons.[25] On one hand, 1D infinite chain-type synthons can be formed via a single hydrogen bond between two carboxylic groups, and such chains incline to crystallize, which can be incorporated in the structures with extended polymeric anions.[26] On the other hand, centrosymmetric dimer-type synthons constructed with H-bonding pairs between two carboxylic groups are much more common. According to the results of single-crystal X-ray diffraction analysis, compound **3** crystallizes in the triclinic space group of $P\bar{1}$. The repeat unit of $BiI_4^-$ in the asymmetry unit is charge-balanced by the monovalent cation of *trans*-4-(aminomethyl)-cyclohexane-carboxylic acid. $BiI_6$ octahedra in **3** are linked together in the edge-shared mode to form infinite chains along the *a* axis (Figure 7a). These anionic chains are stabilized by the pseudodications of *trans*-4-(aminomethyl)-cyclohexane-carboxylic acid pairs, which are formed through the H bonds between two carboxylic groups (Figure 7b, centrosymmetrical synthon). The cyclohexane ring adopts the most stable conformation

(25) Moulton, B.; Zaworotko, M. J. *Chem. Rev.* **2001**, *101*, 1629.
(26) Mercier, N. *CrystEngComm* **2005**, *7*, 429.

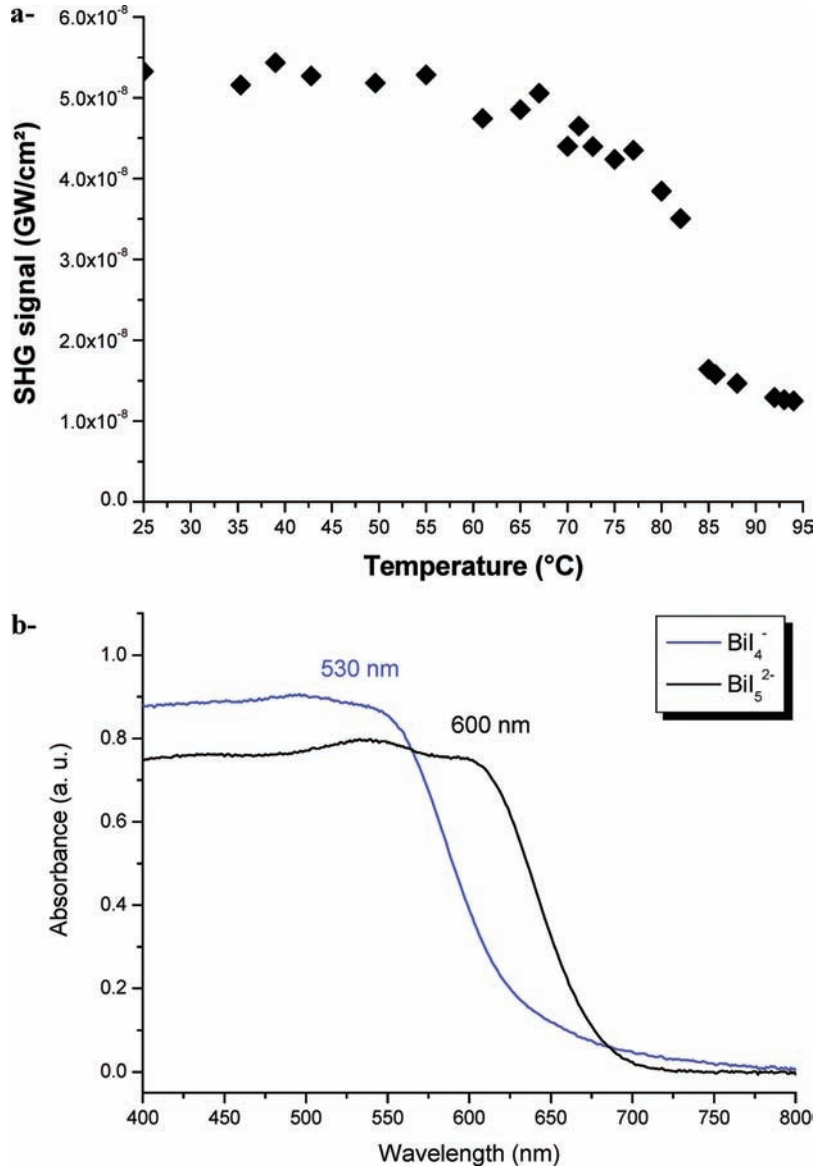


**Figure 6.** (a) SHG signal of a crystalline sample of **1a** driven by temperature. (b) UV−vis spectra of **1a** ("$BiI_5$ chains") and **3** ("$BiI_4$ chains").

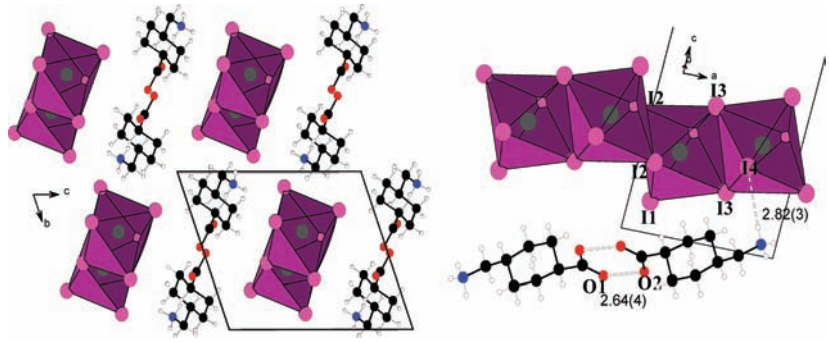


**Figure 7.** The structure of **3**. (a) General view along a; (b) the supermolecular cationic entity resulting from the hydrogen-bonding self-assembling of two molecules, which are hydrogen-bonded to one terminal iodide of the $BiI_4$ chain.

of the chair mode, and the carboxylic group and the aminomethyl group are located in the equatorial direction. The central $Bi^{3+}$ ion is coordinated by six I atoms to form a slightly distorted octahedron, which shows angular deviations from the ideal of < 7° ($I_2-Bi_1-I_3 = 83.13°$, $I_1-Bi_1-I_2 = 95.77°$). The Bi−I bonds in the octahedron range from 2.924 to 3.300 Å with an average of 3.105 Å, among which the bridged Bi−I bonds are much longer than the terminal ones, as observed for such a 1D chain.[13] The $-NH_3^+$ groups are oriented toward terminal iodides, the shortest N−I distance being 3.638 Å, which indicates that there are quite strong H bonds between them. The

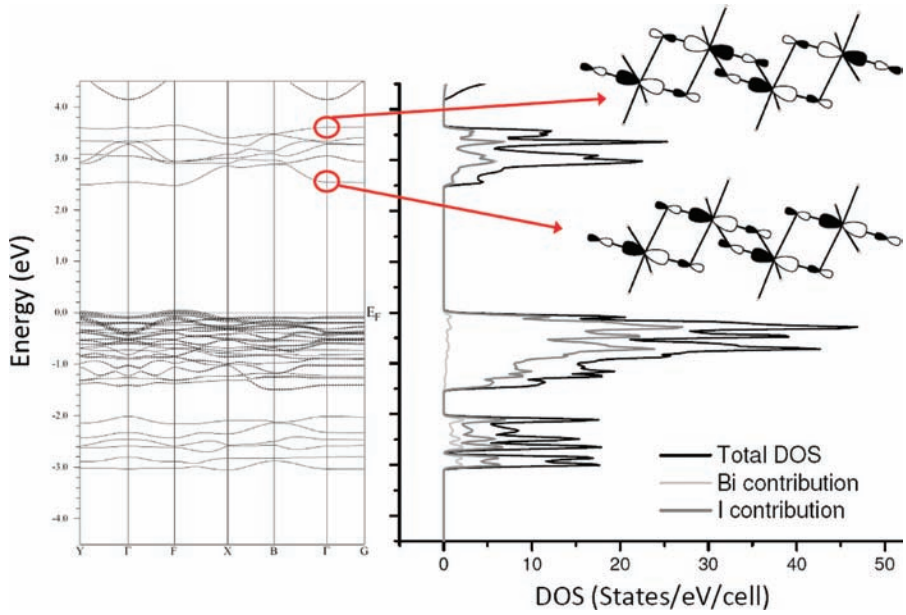


**Figure 8.** Band structure of **3** and corresponding total DOS and partial DOS (bismuth and iodine). The contribution of the Bi 6s levels into the wave function is shown as fat band evolution. Orbital scheme of $\sigma^*$ interactions at the bottom and top of the CB is shown on the right-hand side.

shortest distance between two I atoms from the adjacent chains is 4.272 Å, which is a common value in such salts.

**Electronic Band Structure Calculations and Discussion.** For all of the compounds under investigation, the electronic properties (gap and mobility) are roughly imposed by the inorganic parts, while the cationic organic entities can influence the geometry of the inorganic frameworks. So, having found a way to properly describe the charge of organic cations (see the Experimental Section and ref 5), the chemical bond analysis can be done keeping only the inorganic component. The full potential WIEN2k code, known as a reference in DFT-based band structure calculations, has been used for this purpose.

The band structure calculated along high symmetry lines (see ref 24 for labels) for compound **3** and the corresponding total DOS and partial DOS (bismuth and iodine) are given Figure 8. A direct gap of 2.5 eV is calculated at point F (0 1/2 0). Considering the following ionic salt $(HO_2C(C_6H_4)\text{-}CH_2NH_3)^+(BiI_4)^-$ and keeping in mind an ionic picture, $Bi^{III}(6s^{26}p^0)/I^{-I}(5s^{25}p^6)$, the main features of the band structure can be interpreted. The valence band (VB) originates mainly from the iodine 5p states, the lower part being stabilized due to $\sigma$ bonding interactions with the bismuth 6p states. The main contribution in the conduction band (CB) comes from the bismuth 6p states, and the presence of $\sigma^*$ antibonding interactions with iodine 5p states is visible in Figure 8. We should notice that the CB presents a rather low dispersion and spans a quite small energy range (1.2 eV), contrary to what was observed for the CB built with a 6p band of lead in ref 5 (2D $PbI_4$ perovskite layer), where a width of about 3.4 eV was found. In fact, the $\sigma^*$ interaction is present with nearly the same amplitude all over the CB and whatever the *k* point of the Brillouin zone. In the 2D perovskite layer, for instance, the strength of the $\sigma^*$ interaction changes a lot from nil at the bottom of the CB to a maximum at the top. Thus, due to the specific octahedron arrangement in compound **3** (zigzag chains of edge-shared octahedra), the separation between those $\sigma^*$ levels mainly comes from the presence of $\pi$ or $\pi^*$ interactions (see the orbital schemes on the right-hand side of Figure 8). It explains the small width of the CB.

Let us now have a look at the top of the VB, where one expects the presence of $\sigma^*$ interaction between the iodine p states and the bismuth 6s lone pair. The participation of the Bi 6s states in the wave function is shown as fat bands on the band structure (Figure 8). We should remember that, for 2D perovskite, this interaction is responsible for the dispersion of the last occupied valence states,[4,5] and expecting larger carrier mobility, we are looking for more dispersed states close to the Fermi level. In the present compound, the iodine p states concerned with this $\sigma^*$ interaction are not very well separated from others and present a rather low dispersion. In fact, due to geometry frustrations in relation with the specific octahedron arrangement, the Bi 6s orbital cannot present perfect $\sigma^*$ interactions with all six surrounding iodine atoms. As a consequence, the antibonding interaction is not too strong and the band dispersion is rather small. This frustration can be observed when drawing an isosurface of the charge density calculated from the square modulus of the highest occupied wave function obtained at F (see Figure VI-D in the Supporting Information). The nonspherical contribution of the Bi 6s orbital clearly shows the lone pair stereoactivity in accordance with the Bi site distortion.

We will now focus on compound **1**, which still has a 1D zigzag chain of $BiI_6$ octahedra but presents a significantly lower absorption edge (1.9 eV) compared to **3** (2.1 eV), as determined from the lower energy absorption band in the UV−vis spectra of **1a** and **3** (Figure 6b). In **1a**, the octahedron connection is now through corners instead of edges for compound **3**, and this affects the band structure. We will show, however, that it is not the only reason for the band gap reduction. The band structure of **1** is given in Figure

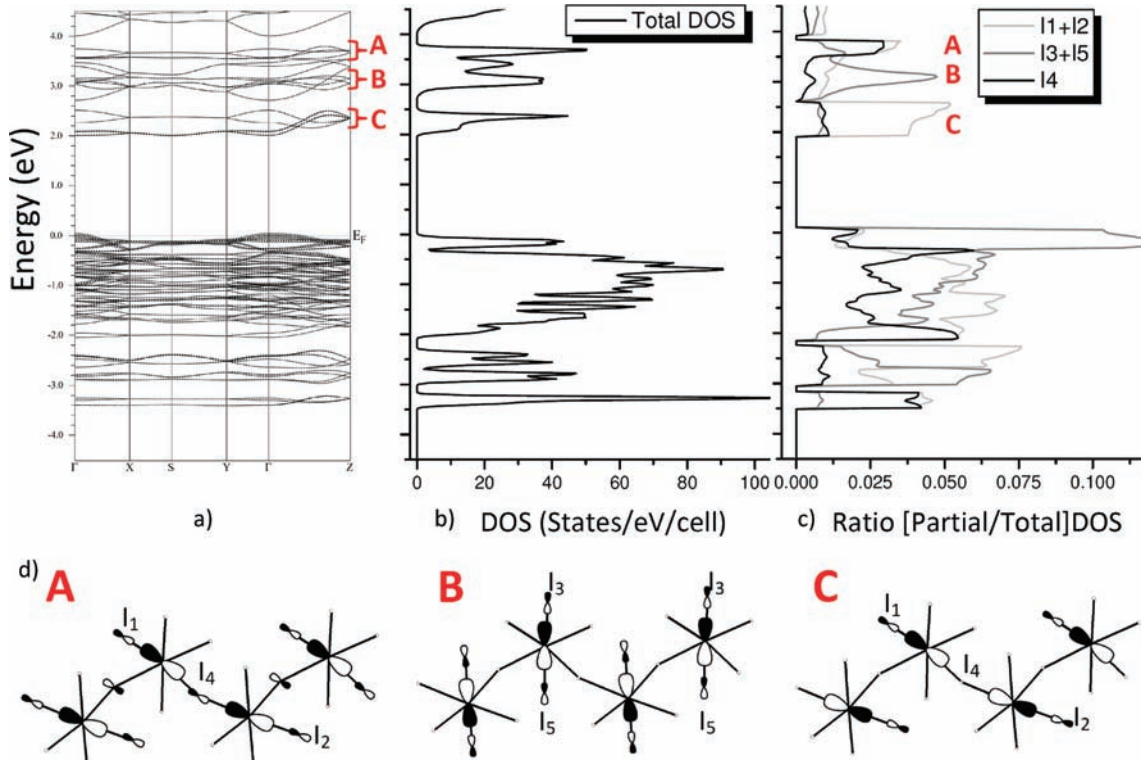


**Figure 9.** Band structure of **1** (a), corresponding total DOS (b), DOS relative contribution of iodine atoms (c), and orbital schemes of $\sigma^*$ interactions in the CB (d).

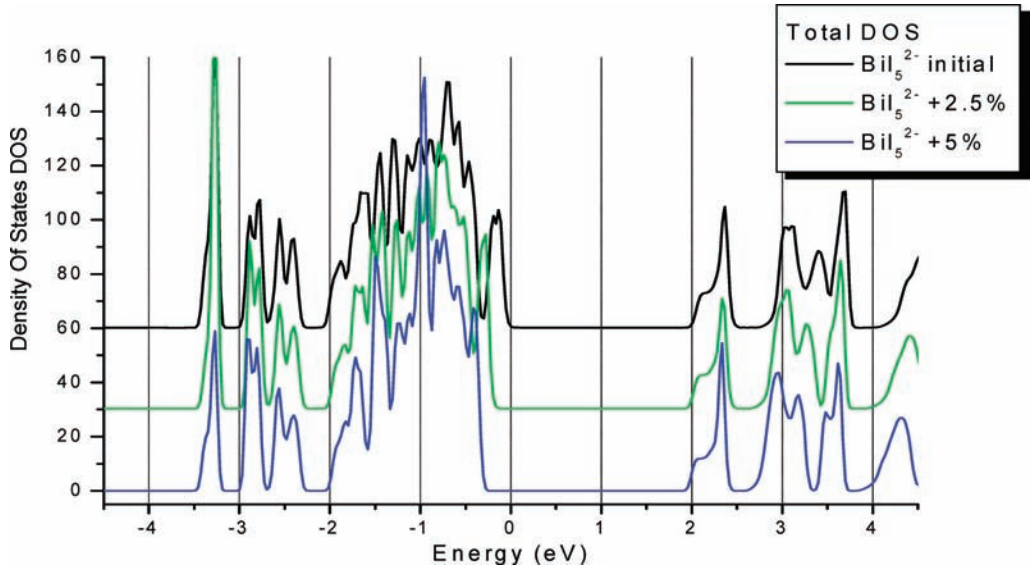


**Figure 10.** Total DOS for **1a** (up) and derived compounds **1a2.5** (middle) and **1a5.0** (down) (see text for explanation about **1a2.5** and **1a5.0** compounds).

9a together with the total DOS (Figure 9b). A direct gap of 2.0 eV is calculated for this compound, quite in agreement with the reduction expected from experiments. As a first observation, we should notice that, while the CB still presents a small dispersion, its bandwidth (∼1.8 eV) is greater compared to **3** (∼1.2 eV). Regarding the partial DOS ratio plotted in Figure 9c for the various iodine contributions, apical (I3+I5), equatorial but not shared between two octahedrons (I1+I2) and finally I4, which is the bridging atom (see Figure 9d for the labels), one can isolate three distinct interactions in the CB. The lowest states (C) involve only one $\sigma^*$ interaction per bismuth with the nonbridging equatorial iodine atoms (I1 and I2). The intermediate bloc (B) corresponds to two $\sigma^*$ interactions per bismuth with the apical atoms I3 and I5, and finally, all of the equatorial atoms (I1, I2, and I4) contribute to the most antibonding states (A). This is schematically illustrated in the lower part of Figure 9. The bandwidth of the CB being increased compared to **3**, this can explain part of the gap reduction.

Looking now at the top of the VB, one finds, opposite to **3**, iodine p levels that are well-separated from others due to the $\sigma^*$ interactions with the bismuth 6s states. These $\sigma^*$ interactions, that push the iodine p states higher in energy, imply mainly apical I3 and I5 atoms with also rather small

contributions coming from the equatorial atoms. The frustration that was in fact observed in **3**, limiting the importance of the $\sigma^*$ I-p/Bi-s interaction, is partially removed with the corner-shared connection. This point is also in favor of the gap reduction. In our chemical bond description, we have however completely ignored the interchain interactions, but we have shown previously that those I−I distances are quite small (less than 4 Å), at least much smaller than the sum of van der Waals radii of two I atoms (4.3 Å). In order to evaluate the effect of those interchain interactions on the band structure, we have calculated the band electronic structure of the two **1a2.5** and **1a5.0** models, on the basis of the **1a** structure but containing larger interchain I−I distances (see the Experimental Section for the model description). The comparison of the three band structures are given as Supporting Information, while the total DOSs of **1a**, **1a2.5**, and **1a5.0** are compared in Figure 10. As the geometry of the chains is the same in the three structures, the $\sigma$ I-p/Bi-p interaction is expected to be the same. So, we choose to define the bottom of the VB as an energy reference. Comparing the three band structures, we can conclude that this reference is sensible, as many bands are not at all affected by the increase of the interchain distances: see for instance all of the $\sigma$ (or $\sigma^*$) I-p/Bi-p interactions in the VB (or CB). Drastic changes are only visible in the upper part of the VB (between −2 eV and the Fermi level), the bandwidth decreasing from ∼2 eV for **1** to ∼1.7 eV for **1a5.0**. Thus, we can conclude that the interchain interactions are responsible for a reduction of about 0.2 eV of the electronic gap. We have here a very important key point for those types of compounds: the possibility to adjust the electronic gap by replacing the organic cation in order to modify the interchain distances.

## Conclusion

In summary, the peculiar asymmetrical dication of dmes has been incorporated in iodometallate(III) hybrids. An acentric polar iodobismuthate salt based on cis-corner-shared octahedra, namely, α-(dmes)$BiI_5$ (**1a**), is obtained, and interestingly, a single-crystal-to-single-crystal process occurs at moderate temperatures ($T = 70$ °C), leading to the acentric apolar $\beta$ phase (**1b**). This reversible polar-to-apolar transition is explained by an unexpected umbrella reversal of sulfonium groups in the solid state together with a conformational change of $BiI_5$ chains. In accordance with its polarity, the SHG signal intensity generated by **1a** is stronger than the one of **1b**. Another impact of the dmes dications on the structure of **1a** is the shortening of I···I interchain distances ($d_{I...I} < 4$ Å), which modulates the electronic properties of hybrids, as quantified by DFT calculations. Calculations on 1D $BiI_5$ (**1a**) and 1D $BiI_4$-based structures also shows that the narrower band gap in the $BiI_5$ compound appears to be associated with a $\sigma^*$ I-p/Bi-s interaction that moves the Fermi level to higher energy.

**Acknowledgment.** The calculation presented in this work has been carried out at the "Centre Régional de Calcul Intensif des Pays de la Loire" (CCIPL), financed by the French Research Ministry, "The Région Pays de la Loire", and Nantes University. We gratefully acknowledge J. Luc for SHG measurements.

**Supporting Information Available:** Crystallographic data: single crystal results (CIF) and powder X-ray patterns for **1a** (= $f(T)$), **1b**, **2**, and **3**; thermal analysis (TGA, DSC) data; UV−vis spectra; and model compounds' input files (CIF). This material is available free of charge via the Internet at http://pubs.acs.org.

IC801900R